LETTER

doi:10.1038/nature12233

Structural basis for alternating access of a eukaryotic calcium/proton exchanger

Andrew B. Waight[1], Bjørn Panyella Pedersen[1], Avner Schlessinger[2], Massimiliano Bonomi[2], Bryant H. Chau[1], Zygy Roe-Zurz[1], Aaron J. Risenmay[1], Andrej Sali[2] & Robert M. Stroud[1]

Eukaryotic Ca^{2+} regulation involves sequestration into intracellular organelles, and expeditious Ca^{2+} release into the cytosol is a hallmark of key signalling transduction pathways. Bulk removal of Ca^{2+} after such signalling events is accomplished by members of the Ca^{2+}:cation (CaCA) superfamily[1–5]. The CaCA superfamily includes the Na^{+}/Ca^{2+} (NCX) and Ca^{2+}/H^{+} (CAX) antiporters, and in mammals the NCX and related proteins constitute families SLC8 and SLC24, and are responsible for the re-establishment of Ca^{2+} resting potential in muscle cells, neuronal signalling and Ca^{2+} reabsorption in the kidney[1,6]. The CAX family members maintain cytosolic Ca^{2+} homeostasis in plants and fungi during steep rises in intracellular Ca^{2+} due to environmental changes, or following signal transduction caused by events such as hyperosmotic shock, hormone response and response to mating pheromones[7–13]. The cytosol-facing conformations within the CaCA superfamily are unknown, and the transport mechanism remains speculative. Here we determine a crystal structure of the *Saccharomyces cerevisiae* vacuolar Ca^{2+}/H^{+} exchanger (Vcx1) at 2.3 Å resolution in a cytosol-facing, substrate-bound conformation. Vcx1 is the first structure, to our knowledge, within the CAX family, and it describes the key cytosol-facing conformation of the CaCA superfamily, providing the structural basis for a novel alternating access mechanism by which the CaCA superfamily performs high-throughput Ca^{2+} transport across membranes.

The CaCA superfamily is defined by the presence of two short, repeating homologous sequences, termed the α-repeats, found in predicted transmembrane regions. The α-repeats are opposite in topology and are believed to have arisen from a gene duplication event[14–16]. Mutagenesis and recent structural data have identified this region as essential for ion binding and transport, and specifically two key acidic residues (Glu or Asp) are implicated in coordinating Ca^{2+} ions at the active site[17–20]. Members of the CAX family are approximately 400 residues long with 11 predicted transmembrane helices. The first helix (MR), found in eukaryotic CAX members, has a regulatory role in plant members and is suggested to be involved in protein targeting and/or signalling in yeast[12,21,22]. The 10 remaining transmembrane helices (M1–M10) perform the transport function, and are composed of two symmetrically related halves (M1–M5 and M6–M10) connected through a negatively charged loop termed the 'acidic motif'[12,16,23]. *Saccharomyces cerevisiae* Vcx1 catalyses low-affinity (Michaelis constant (K_m) = ~25 μM), high-capacity (maximum rate (V_{max}) = ~35 nmol Ca^{2+} min^{-1} mg^{-1}) vacuolar Ca^{2+} exchange[3,8,24,25]. To establish function of the purified protein, Vcx1 was reconstituted into liposomes and assayed for Ca^{2+} uptake activity. In this system, purified Vcx1 demonstrates Ca^{2+} uptake monotonically dependent on pH gradient (Supplementary Fig. 1). Vcx1 shares ~30% sequence identity with other members of the Ca^{2+}/H^{+} exchanger family, including the canonical CAX proteins of *Arabidopsis thaliana* (Supplementary Fig. 2).

Vcx1 was solved experimentally to 2.3 Å resolution (R_{free} of 22.5%) by molecular replacement, supported by iodine-based experimental phases (Fig. 1, Supplementary Table 1 and Supplementary Fig. 3). The structure encompasses residues 22–401 with the exception of a short loop (184–191) between M4 and M5. Two identical (root mean squared deviation (r.m.s.d.) 0.21 Å over 285 Cα atoms) monomers are found in the asymmetric unit. Six divalent cations are identified as Ca^{2+} or Mn^{2+} in the Vcx1 monomer, on the basis of their coordination geometry and anomalous scattering differences (Supplementary Fig. 4).

The shape of the VCX monomer, viewed perpendicular to the membrane plane, resembles that of a wedge (Fig. 1). Viewed from the vacuolar side of the membrane, the tapered end of the wedge consists of two long antiparallel helices M1 and M6, which are intertwined and tilted ~30° with respect to the membrane normal. The central four-helix core contains the α-repeats, and is comprised of M2–M3 and M7–M8. M2 and M7 are kinked at their midpoints and change direction ~35° in the middle of the membrane plane to create M2a/M2b and M7a/M7b. These two oppositely related helix kinks meet in the mid-membrane plane, forming an hourglass shape, where the CAX family display the conserved GNXXE(H) signature sequence necessary for calcium binding and transport[19,20,26,27]. M3 and M8 are also tilted with respect to the membrane normal and line the interior of the hourglass. M4–M5 and M9–M10 form the outer components of a right-handed bundle which flank the central core and constitute the thicker side of the wedge shape. The 20-residue 'acidic motif' connecting the two duplicated halves of the protein between M5 and M6 is predicted to be disordered based on sequence. However, a clearly resolved α-helix (which we term the acidic helix) for this sequence is observed in the structure. This helix is oriented parallel to the membrane and lies directly underneath the α-repeat regions on the cytosolic side.

A centrally located Ca^{2+} ion occupies the active site of Vcx1, coordinated by Glu 302 on M7b and Ser 325 on M8 (Fig. 2). The Ser 325 residue is generally conserved throughout the CaCA superfamily, and in NCX and NCKX family members the analogous serine residue has been shown to have an important role in Ca^{2+} transport (Supplementary Fig. 5)[18,19]. Three ordered water molecules complete the octahedral coordination geometry of Ca^{2+} (Supplementary Fig. 4b). The presence of water molecules at the binding site suggest that the Ca^{2+} ion reaches the active site in a partially hydrated state, balancing the stronger binding of entropically ordered side chains with more loosely bound water to complete the coordination sphere. Glu 106, Asn 299 and the backbone carbonyl of Gly 102 coordinate the three water molecules. The remainder of the Ca^{2+} active site is stabilized by specific interactions from polar residues in the transmembrane regions of M2, M3, M7 and M8. The conserved Asn 299 and His 303 of M7b form a hydrogen bond to Ser 129 and Ser 132, respectively, of the adjacent M3 helix, and the conserved Asn 103 on M2b forms a hydrogen bond to Gln 328 on M8. M2a is bent away from the bundle of helices M2b, M3, M7 and M8, and in this configuration it is not packed tightly against the protein body (Fig. 3). M2a and the connected C-terminal half of M1 are bent away from the active site, exposing the central Ca^{2+} ion to the cytosol. The M2a/M1 arrangement creates a substantial

[1]Department of Biochemistry and Biophysics, University of California, San Francisco, California 94158, USA. [2]Department of Bioengineering and Therapeutic Sciences, Department of Pharmaceutical Chemistry, California Institute for Quantitative Biosciences, University of California, San Francisco, California 94158, USA.

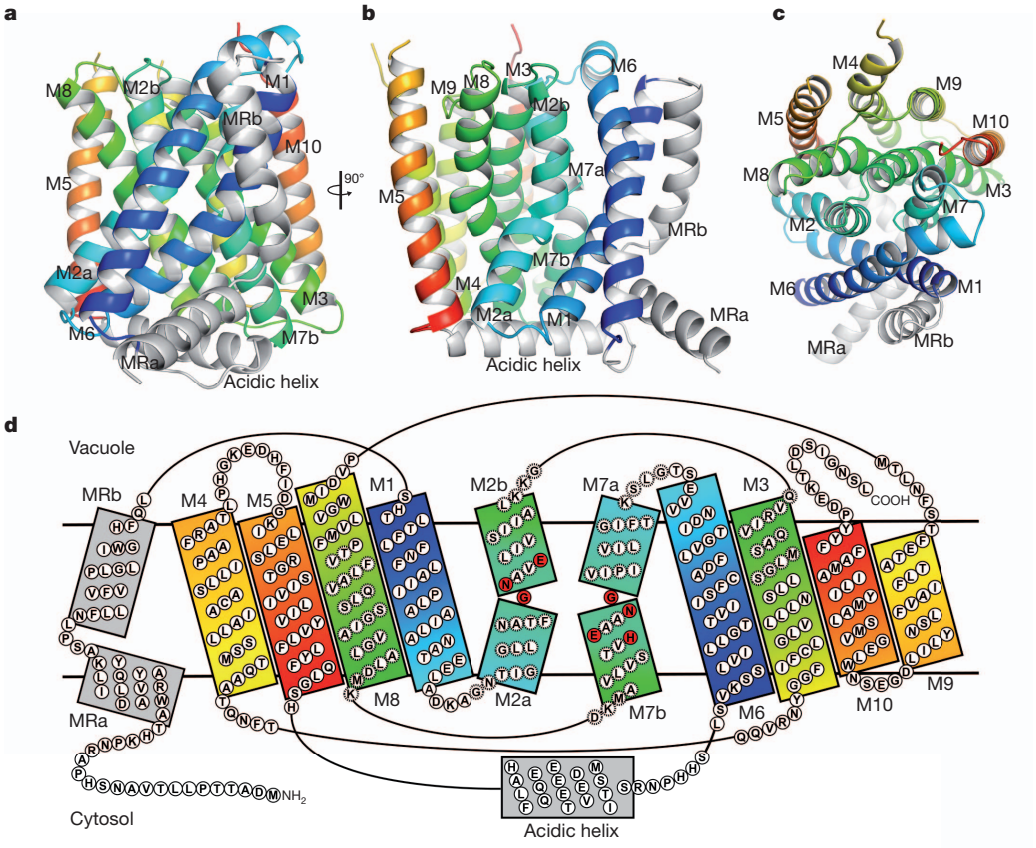

Figure 1 | Topology and fold of the Vcx1 protein. The symmetrically related halves of the Vcx1 monomer are coloured in a double colour spectrum from the N to C terminus. Helices of matching colour are related by symmetry. **a**–**c**, The Vcx1 monomer as viewed in the membrane along the axis of symmetry (**a**), rotated by 90° (**b**) and viewed from the vacuolar side of the membrane (**c**). **d**, Topology map of the Vcx1 monomer; CAX family conserved residues are coloured in red, α-repeat sequences are denoted by dashed circles.

vestibule that is accessible from the intracellular bulk solvent. This vestibule is conical in shape and has a negatively charged interior surface potential (Fig. 3c). The interior of the cavity vestibule is circumscribed by M2a, the C-terminal half of M1, M7b and the N-terminal half of M8, and allows access from the cytosol to the central Ca^{2+} binding site. Thus, the Vcx1 protein structure represents a substrate-bound, cytosol-facing conformation.

Lying across the cytosolic entrance to the vestibule, the acidic helix also coordinates two Ca^{2+} ions (Supplementary Fig. 4c). These two ions lie on the cytosolic side, 11 Å from the central Ca^{2+} site, coordinated by Asp 234 and Glu 230 of the acidic helix and by Glu 83 of M1 (Fig. 2c). The acidic motif has been suggested to have a role in Ca^{2+} binding[23]. In mammalian NCX members, the analogous region connecting helices M5 and M6 contains a large intracellular calcium-binding domain (CBD1) responsible for stimulating activity in the transporter domain in the presence of Ca^{2+} (ref. 28) (Supplementary Fig. 5). The CBD1 Ca^{2+} binding sites are similarly formed from acidic motifs although they coordinate ions using β-sheets rather than α-helical secondary structures[29]. Molecular dynamics simulations performed with the Vcx1 structure suggest that the acidic helix maintains an α-helical conformation in the presence of the two coordinated Ca^{2+} ions, and becomes more flexible in their absence (Supplementary Fig. 6). The increased rigidity of the Vcx1 acidic helix at higher Ca^{2+} concentrations indicates a possible Ca^{2+}-dependent regulatory

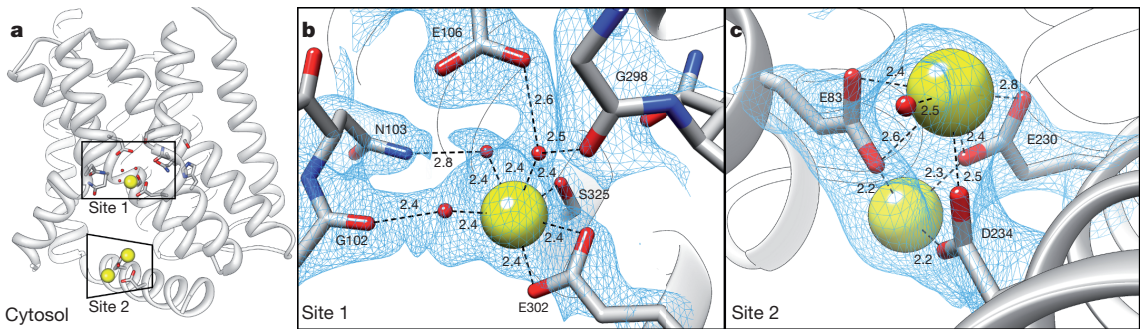

Figure 2 | Calcium binding sites in the Vcx1 crystal structure. **a**, Overview of site 1 and site 2 with helices MR, M1 and M6 removed for clarity. The cytosol is on the bottom of the image and Ca^{2+} ions are coloured in yellow. **b**, Active site Ca^{2+} substrate ion and interacting residues found in site 1. Hydrogen bonds are shown as dashed lines; numbers denote atomic distances (Å). $2mF_o - DF_c$ map is shown contoured at 1σ (blue mesh). **c**, Ca^{2+} ions at the acidic helix in site 2 with interacting residues labelled. Hydrogen bonds are shown as dashed lines; numbers denote atomic distances (Å). $2mF_o - DF_c$ map is shown contoured at 1σ (blue mesh).

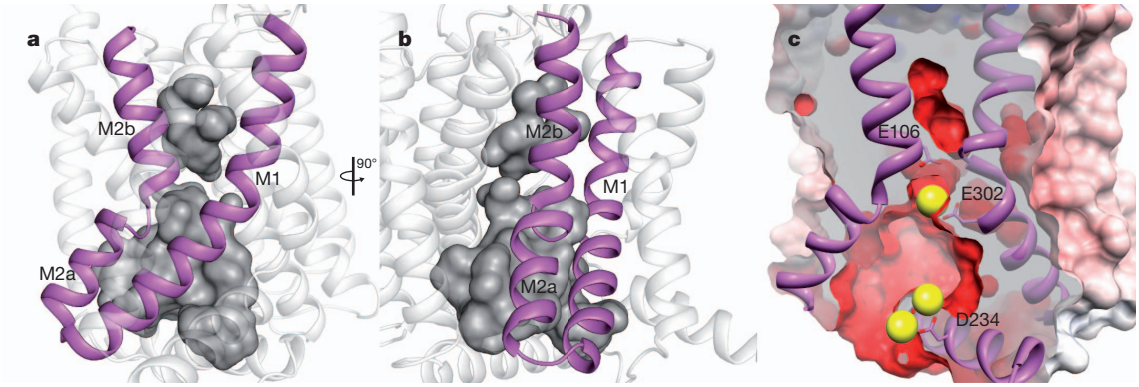

Figure 3 | The cytoplasmic vestibule. **a**, The protein cavity is rendered as a surface representation and is coloured grey; the helices M1 and M2 are coloured purple and are shown from the axis of symmetry. **b**, View rotated by 90°. **c**, The cytoplasmic vestibule as oriented in panel **a** and depicted with a slab surface representation coloured by electrostatic potential (red to blue; −10 to 10 kT e^{-1}). Helices MR, M1 and M6 have been removed for clarity. Ca^{2+} ions (yellow spheres) pinpoint site 1 and site 2.

function for this region, perhaps augmenting conductance in the presence of increased cytosolic Ca^{2+}.

Comparison of the two structural repeats (M1–M5 and M6–M10) of Vcx1 reveals a structurally similar core region that is closely packed and rigid (M3–M5, M8–M10) (Supplementary Fig. 7b). In contrast, considerable differences are found in the M2a helix and C-terminal half of M1 when compared to M7a and M6. Superposition between helices M1–M2a and M6–M7a reveal a ~12° and ~7° asymmetric difference in the angle of M1 and M2a, respectively (Supplementary Fig. 7c, d). This structural divergence, in combination with loose packing and intracellular location, implicate this mobile region as the cytosolic gate. A dynamic straightening of the M1/M2a helices would collapse the cytosolic vestibule, and this motion could be coordinated by a structural rearrangement into a vacuole-facing conformation.

The Vcx1 conformation also sheds light on the transport cycle of CaCA proteins by comparison with the recent structure of an archaebacterial Na^{+}/Ca^{2+} exchanger from *Methanococcus janaschii* (mjNCX)[17]. Despite low sequence identity (14%) to Vcx1, the overall fold and topology of mjNCX is similar. However, unlike Vcx1, the mjNCX exchanger is closed to the cytosolic environment and instead represents a periplasm-facing conformation, as reflected in the overall displacement between similar atoms (r.m.s.d. 5.7 Å over 269 Cα atoms). Structural alignment of the Vcx1 and mjNCX structures reveals a similar placement of the core region and of helices M7 and M2b (Supplementary Fig. 8). However, the M2a helix is shifted by ~16 Å towards the centre of the bilayer in Vcx1 (Fig. 4a). In addition, relative to the mjNCX structure, the position of both loosely packed helices M1 and M6 are translated diagonally towards the vacuole by ~16 Å and ~13 Å at either end, closing a vacuole-facing portal that could otherwise expose the active site of the protein to the vacuolar environment (Fig. 4b and Supplementary Figs 8 and 9). The concerted transposition in the M1/M6 helices therefore performs a dual role of coordinating motions between the α-repeats and covering/uncovering an active site entry passage (Fig. 4c). By this mechanism, translational movements of the M1/M6 helices allow alternating access to the active site of Vcx1 from both sides of the membrane. The action of the M1/M6 helices is therefore analogous to the piston of a two-stroke engine that occludes and exposes intake and efflux pathways during each turnover. Using a predicted cytosol-facing mjNCX conformation, a similar motion of the M1 and M6 helices was suggested for turnover by the mjNCX monomer[17]. Our data augment the proposed mechanism by including structural evidence for the M1/M6 translations and substantial conformational changes in the M2a helix. With the addition of a cytoplasmic-facing Vcx1 structure, there are now two key states in the CaCA family that suggest a trajectory for Ca^{2+} translocation, forming a strong case for the two-stroke mechanism of alternating access.

The proposed transport cycle of Vcx1 is shown in Fig. 4c (Supplementary Video 1). In the active site, Glu 106 and Glu 302 are exposed to the vacuolar side (pH ~5–6 (ref. 30)). The proton motive gradient across the vacuolar membrane provides the source of energy to drive a conformational change to the cytosol-facing conformation whereupon the glutamate residues would be expected to maintain a negative charge (at pH ~7 (ref. 30)). Under conditions of high cytosolic Ca^{2+} concentration, as seen during signal transduction events,

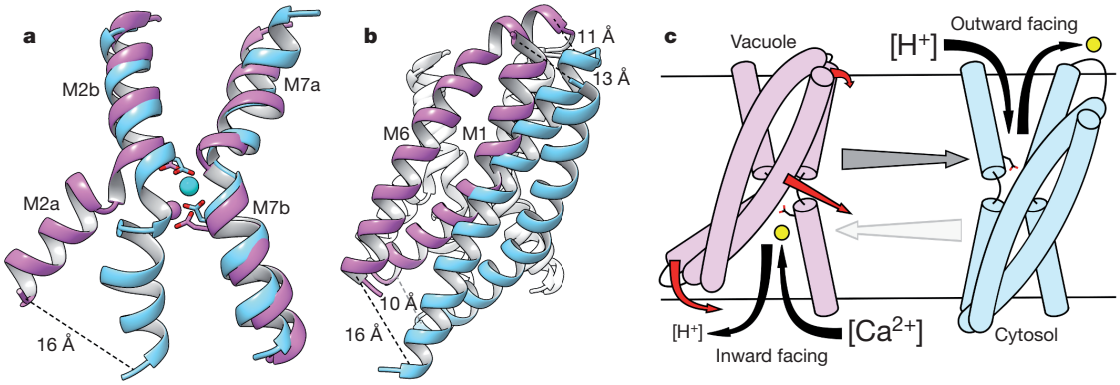

Figure 4 | Transport cycle of Vcx1 and structural comparison to mjNCX. **a**, Comparison of M2 and M7 and active site glutamate residues between Vcx1 (purple) and mjNCX (cyan). Ca^{2+} ions from each model are depicted as spheres. **b**, Comparison of M1 and M6 between Vcx1 (purple) and mjNCX (cyan). **c**, Schematic of Vcx1 turnover. Structures are coloured as in panel **a**. Proposed substrate movement is denoted by black arrows, and calcium by yellow circles. Red arrows show protein movement in the cytosol-facing state of Vcx1 (left) that results in the vacuole-facing conformation on the right. Return to the cytosol-facing state presumably requires reversal of the movements denoted by the red arrows.

Ca^{2+} is coordinated by the acidic helix, and Ca^{2+} is able to reach the active site. The Vcx1 side chains of Glu 302 and Ser 325 partially replace the Ca^{2+} hydration shell, and subsequent completion of coordination by Glu 106 displaces some of the remaining water molecules to bring helix M2b inward towards the active site. This movement of M2 towards the core can initiate M2a straightening and M1/M6 translation, closing the cytosolic vestibule. The translation of helices M1/M6 uncovers a vacuolar cleft and coordinates opening of M7a to expose the active site Ca^{2+} ion to the vacuole. The vacuole-facing conformation, in combination with the acidic pH in the vacuole, lowers the Ca^{2+} affinity of active site residues Glu 106 and Glu 302, leading to release of the Ca^{2+} substrate into the vacuole. The cyclical pumping action of the M1/M6 'piston', coupled to flexible helices surrounding the active site (M2a, M7a), provides an efficient framework for the rapid turnover necessary for high-throughput Ca^{2+} exchange.

In conclusion, Vcx1 is the first CAX family structure, and the first structure of the CaCA superfamily in a cytosol-facing conformation. It provides a structural basis for an alternating access mechanism for the Vcx1 protein and the CaCA superfamily in general. These findings lay the groundwork for future exploration of Ca^{2+} transport by CaCA superfamily members and lend insight into fundamental aspects of Ca^{2+} homeostasis and eukaryotic signal transduction processes.

METHODS SUMMARY

The Vcx1 protein from *Saccharomyces cerevisiae* (Uniprot ID Q99385) was expressed in *S. cerevisiae* and purified using a decahistidine affinity-tag. Solubilization and purification were performed using dodecyl-β-D-maltoside. Crystals were grown in-meso by combining lipidic cubic phase technique and Jeffamine M-600 sponge phase conditions with vapour phase diffusion. X-ray diffraction was collected at the Advanced Light Source beamline 8.3.1, Advanced Photon Source beamline 23-ID-B and Stanford Synchrotron Radiation Lightsource beamline 12-2. The structures were solved by single-wavelength anomalous diffraction and molecular replacement methods (MR-SAD) using mjNCX (Protein Data Bank accession 3V5U (ref. 17)) as a search model. The final structural model was refined using data to 2.3 Å to a crystallographic *R*-factor of 20.1% and free *R*-factor of 22.5% (Supplementary Table 1).

Full Methods and any associated references are available in the online version of the paper.

Received 5 November 2012; accepted 30 April 2013.
Published online 19 May 2013.

1. Crespo, L. M., Grantham, C. J. & Cannell, M. B. Kinetics, stoichiometry and role of the Na-Ca exchange mechanism in isolated cardiac myocytes. *Nature* **345,** 618–621 (1990).
2. Cui, J. *et al.* Simulating calcium influx and free calcium concentrations in yeast. *Cell Calcium* **45,** 123–132 (2009).
3. Miseta, A., Kellermayer, R., Aiello, D. P., Fu, L. & Bedwell, D. M. The vacuolar Ca^{2+}/H^{+} exchanger Vcx1p/Hum1p tightly controls cytosolic Ca^{2+} levels in *S. cerevisiae*. *FEBS Lett.* **451,** 132–136 (1999).
4. Philipson, K. D. & Nicoll, D. A. Sodium-calcium exchange: a molecular perspective. *Annu. Rev. Physiol.* **62,** 111–133 (2000).
5. Nicoll, D. A., Longoni, S. & Philipson, K. D. Molecular cloning and functional expression of the cardiac sarcolemmal Na^{+}-Ca^{2+} exchanger. *Science* **250,** 562–565 (1990).
6. Lytton, J. Na^{+}/Ca^{2+} exchangers: three mammalian gene families control Ca^{2+} transport. *Biochem. J.* **406,** 365–382 (2007).
7. Hirschi, K. D., Zhen, R. G., Cunningham, K. W., Rea, P. A. & Fink, G. R. CAX1, an H^{+}/Ca^{2+} antiporter from *Arabidopsis*. *Proc. Natl Acad. Sci. USA* **93,** 8782–8786 (1996).
8. Pozos, T. C., Sekler, I. & Cyert, M. S. The product of HUM1, a novel yeast gene, is required for vacuolar Ca^{2+}/H^{+} exchange and is related to mammalian Na^{+}/Ca^{2+} exchangers. *Mol. Cell. Biol.* **16,** 3730–3741 (1996).
9. Cheng, N.-H., Pittman, J. K., Barkla, B. J., Shigaki, T. & Hirschi, K. D. The *Arabidopsis cax1* mutant exhibits impaired ion homeostasis, development, and hormonal responses and reveals interplay among vacuolar transporters. *Plant Cell* **15,** 347–364 (2003).
10. Cho, D. *et al.* Vacuolar CAX1 and CAX3 influence auxin transport in guard cells via regulation of apoplastic pH. *Plant Physiol.* **160,** 1293–1302 (2012).
11. Cunningham, K. W. Acidic calcium stores of *Saccharomyces cerevisiae*. *Cell Calcium* **50,** 129–138 (2011).
12. Shigaki, T., Rees, I., Nakhleh, L. & Hirschi, K. D. Identification of three distinct phylogenetic groups of CAX cation/proton antiporters. *J. Mol. Evol.* **63,** 815–825 (2006).
13. Denis, V. & Cyert, M. S. Internal Ca^{2+} release in yeast is triggered by hypertonic shock and mediated by a TRP channel homologue. *J. Cell Biol.* **156,** 29–34 (2002).
14. Schwarz, E. M. & Benzer, S. Calx, a Na-Ca exchanger gene of *Drosophila melanogaster*. *Proc. Natl Acad. Sci. USA* **94,** 10249–10254 (1997).
15. Cai, X. & Lytton, J. The cation/Ca^{2+} exchanger superfamily: phylogenetic analysis and structural implications. *Mol. Biol. Evol.* **21,** 1692–1703 (2004).
16. Iwamoto, T. *et al.* Unique topology of the internal repeats in the cardiac Na^{+}/Ca^{2+} exchanger. *FEBS Lett.* **446,** 264–268 (1999).
17. Liao, J. *et al.* Structural insight into the ion-exchange mechanism of the sodium/calcium exchanger. *Science* **335,** 686–690 (2012).
18. Nicoll, D. A., Hryshko, L. V., Matsuoka, S., Frank, J. S. & Philipson, K. D. Mutation of amino acid residues in the putative transmembrane segments of the cardiac sarcolemmal Na^{+}-Ca^{2+} exchanger. *J. Biol. Chem.* **271,** 13385–13391 (1996).
19. Winkfein, R. J. *et al.* Scanning mutagenesis of the alpha repeats and of the transmembrane acidic residues of the human retinal cone Na/Ca-K exchanger. *Biochemistry* **42,** 543–552 (2003).
20. Kang, K.-J. Residues contributing to the Ca^{2+} and K^{+} binding pocket of the NCKX2 Na^{+}/Ca^{2+}-K^{+} exchanger. *J. Biol. Chem.* **280,** 6823–6833 (2005).
21. Pittman, J. K., Sreevidya, C. S., Shigaki, T., Ueoka-Nakanishi, H. & Hirschi, K. D. Distinct N-terminal regulatory domains of Ca^{2+}/H^{+} antiporters. *Plant Physiol.* **130,** 1054–1062 (2002).
22. Pittman, J. K. & Hirschi, K. D. Regulation of CAX1, an *Arabidopsis* Ca^{2+}/H^{+} antiporter. Identification of an N-terminal autoinhibitory domain. *Plant Physiol.* **127,** 1020–1029 (2001).
23. Ivey, D. M. *et al.* Cloning and characterization of a putative Ca^{2+}/H^{+} antiporter gene from *Escherichia coli* upon functional complementation of Na^{+}/H^{+} antiporter-deficient strains by the overexpressed gene. *J. Biol. Chem.* **268,** 11296–11303 (1993).
24. Ohsumi, Y. & Anraku, Y. Calcium transport driven by a proton motive force in vacuolar membrane vesicles of *Saccharomyces cerevisiae*. *J. Biol. Chem.* **258,** 5614–5617 (1983).
25. Dunn, T., Gable, K. & Beeler, T. Regulation of cellular Ca^{2+} by yeast vacuoles. *J. Biol. Chem.* **269,** 7273–7278 (1994).
26. Kamiya, T. & Maeshima, M. Residues in internal repeats of the rice cation/H^{+} exchanger are involved in the transport and selection of cations. *J. Biol. Chem.* **279,** 812–819 (2004).
27. Shigaki, T. *et al.* Identification of a crucial histidine involved in metal transport activity in the *Arabidopsis* cation/H^{+} exchanger CAX1. *J. Biol. Chem.* **280,** 30136–30142 (2005).
28. Matsuoka, S., Nicoll, D. A., Reilly, R. F., Hilgemann, D. W. & Philipson, K. D. Initial localization of regulatory regions of the cardiac sarcolemmal Na^{+}-Ca^{2+} exchanger. *Proc. Natl Acad. Sci. USA* **90,** 3870–3874 (1993).
29. Nicoll, D. A. *et al.* The crystal structure of the primary Ca^{2+} sensor of the Na^{+}/Ca^{2+} exchanger reveals a novel Ca^{2+} binding motif. *J. Biol. Chem.* **281,** 21577–21581 (2006).
30. Martínez-Muñoz, G. A. & Kane, P. Vacuolar and plasma membrane proton pumps collaborate to achieve cytosolic pH homeostasis in yeast. *J. Biol. Chem.* **283,** 20309–20319 (2008).

Supplementary Information is available in the online version of the paper.

Acknowledgements We thank J. Holton, G. Meigs, C. Ogata, N. Venugopalan and T. Doukov for assistance with synchrotron data collection at Advanced Light Source, Advanced Photon Source and Stanford Synchrotron Radiation Lightsource; and C. Waddling and P. Wassam for technical assistance. B.P.P. was supported by a postdoctoral fellowship from the Carlsberg Foundation and later by a fellowship from the Danish Cancer Society; A.S. by NIH grants U54 GM094625 and U01 GM61390; R.M.S. by NIH grants U54 GM094625, GM24485 and GM073210.

Author Contributions A.B.W. optimized the yeast expression system, performed expression, purification and crystallization experiments, collected and processed the data, determined, refined and analysed the structure, and performed reconstitution and transport assays. B.P.P. performed data collection and assisted with structure solution and structural analysis. B.H.C. and A.J.R. assisted in cell collection, membrane preparation and purification experiments. B.H.C. and Z.R.-Z. did cloning and expression tests. A.Sc. constructed Vcx1 comparative models as well as performed bioinformatics and distance plot analysis. M.B. performed molecular dynamics simulations and distance plot analysis. A.B.W., B.P.P. and R.M.S. wrote the paper with input from A.Sc., M.B. and A.Sa.

Author Information Coordinates and structure factors have been deposited in the Protein Data Bank with the accession number 4K1C. Reprints and permissions information is available at www.nature.com/reprints. The authors declare no competing financial interests. Readers are welcome to comment on the online version of the paper. Correspondence and requests for materials should be addressed to R.M.S. (stroud@msg.ucsf.edu).

METHODS

Expression and purification. The Vcx1 protein from *Saccharomyces cerevisiae* (Uniprot ID Q99385) was incorporated into the 2μ expression plasmid p423-GAL1 modified with N-terminal and C-terminal purification tags, as described[31]. Transformed *S. cerevisiae* (strain DSY-5; *MATα his3::GAL1-GAL4 pep4 prb1-1122)* were grown in a fermenter culture vessel (Biostat C15L Sartorius AG) to high density and induction was performed via fed-batch using 40% galactose and harvested after 18–22 h. Harvested yeast (~1.8–2 kg wet cell weight) were washed in cold water, pelleted (6,000 r.p.m.) and flash frozen for storage at −80 °C. Frozen pellets were thawed in lysis buffer (100 mM Tris 7.0, 700 mM NaCl, 1 mM phenylmethylsulphonyl fluoride (PMSF) + protease inhibitors) before cell disruption using a bead mill. The homogenate was centrifuged for 25 min at 21,600*g*, followed by sedimentation of membranes via ultracentrifugation at 185,000*g* for 150 min. Membrane pellets were re-suspended in membrane re-suspension buffer (50 mM Tris pH 7.0, 600 mM NaCl, 20% glycerol) before being frozen in liquid nitrogen in 7-g aliquots. One-hundred grams of yeast cell material yielded an average of 20–25 g membrane. Membrane aliquots (8 g) were thawed and suspended in 112 ml membrane solubilization buffer (50 mM Tris pH 7.0, 600 mM NaCl, 20 mM $CaCl_2$, 10% glycerol 1 mM PMSF + protease inhibitors) and solubilized using 1,380 mg *n*-dodecyl-β-D-maltoside (DDM) (1:0.19 (w/w) ratio) for 30 min at 4 °C, followed by centrifugation at 120,000*g* for 30 min to remove unsolubilized material. The resultant lysate was supplemented with 8 mM imidazole pH 6.5 and incubated for ~3 h with 6 ml pre-equilibrated TALON Co^{2+} resin. After incubation, the beads were collected by gravity flow-through using a Bio-Rad econo-column and washed twice via neutation with 30 ml buffer A (50 mM Tris pH 7.0, 0.1% DDM, 20 mM $CaCl_2$, 5 mM $MnCl_2$, 10% glycerol) supplemented with 15 mM and 30 mM imidazole pH 6.5, respectively. The protein was eluted from the beads using three elutions of 5 ml buffer A supplemented by 500 mM imidazole pH 6.5. The elutions were pooled, bovine thrombin and 3C protease were added to cleave the tags, and dialysed with a 25-kDa cutoff into 1 l of dialysis buffer (50 mM MES pH 6.0, 20 mM $CaCl_2$, 5 mM $MnCl_2$ 10% glycerol) overnight at 4 °C. The following day the eluate was concentrated to 500 μl and injected onto a size-exclusion column (Superdex 200, GE Healthcare) equilibrated SEC buffer (10 mM MES pH 6.0, 0.05% DDM, 20mM $CaCl_2$, 5mM $MnCl_2$). Peak fractions were collected and concentrated to ~30 mg ml^{-1}.

Reconstitution and transport assay. Ca^{2+} uptake into proteoliposomes using purified Vcx1 protein was performed primarily using the method described previously[32]. In brief, 10 mg of yeast polar lipid extract (Avanti Polar Lipids) was dried under nitrogen and re-suspended into 10 mM MOPS pH 6.5, 100 mM choline chloride, and 100 μM Fura-2[33] (Sigma-Aldrich). The re-suspension was sonicated to transparency, subjected to 10 cycles of freeze–thaw, and then extruded through a 400-nm filter 10 times. The resulting liposomes were destabilized by addition of 1% octyl β-D-glycopyranoside (OG) and purified Vcx1 was added in a 1:500 (w/w) ratio and incubated for 1 h. OG was removed by addition of 200 mg ml^{-1} Bio-Beads (Bio-Rad) for 3 h and replaced with 200 mg ml^{-1} fresh Bio-Beads for incubation overnight. Proteoliposomes were harvested by centrifugation at 66,000*g* for 150 min and re-suspended in 10 mM MOPS pH 6.5, 100 mM choline chloride. Proton gradient was initiated by the addition of 20 μl proteoliposome to 20 μl reaction buffer containing 100 mM choline chloride and 10 mM MOPS pH 7.9, 7.2 or 6.5 (final pH 7.1, 6.8. 6.5) in a Corning 384 well clear bottom microplate. Transport activity followed the addition of 100 μM $CaCl_2$, and uptake of Ca^{2+} was monitored at 22 °C via the changes in emission of Fura-2 at 510 nm upon excitation at 340 and 380 nm at 10-s intervals using a Molecular Devices SpectraMax microplate reader. Maximal signal was obtained via addition of 0.3% DDM, the ratio of emission intensities at the two excitation wavelengths was converted to Ca^{2+} using a standard curve and previously described methods[33].

Crystallization. Forty microlitres of concentrated Vcx1 was mixed with 60 μl monoolein to prepare the lipidic cubic phase (LCP) as previously described[34]. Crystals were grown by adding 1 μl Vcx1/LCP mixture to a glass coverslip and overlayed with 2 μl crystallization solution (14% Jeffamine M600 pH 7.0, 100 mM HEPES pH 7.0, 50 mM $CaCl_2$, 50 mM $MnCl_2$, 200 mM NaI). Coverslips were sealed in a hanging-drop setup in 24-well trays containing 300 μl crystallization solution. Crystals appeared in a subsequent sponge phase in approximately 3–4 days and grew to a maximum size of 250 μm. Crystals were harvested from the trays and frozen directly in liquid nitrogen for data collection. Data were collected at Advanced Light Source beamline 8.3.1, Advanced Photon Source beamline 23-ID-B and Stanford Synchrotron Radiation Lightsource beamline 12-2. Holmium heavy-atom derivatives were obtained by adding $Ho(III)Cl_2$ to the crystals 1 h before flash-cooling, either as salt or as a concentrated, aqueous solution.

Data processing. Data sets were processed using XDS[35] in space group *R*3. An initial marginal molecular replacement solution was provided by the mjNCX structure (Protein Data Bank accession 3V5U; 14% identity) using the PHENIX[36] AutoMR program and improved upon by PHENIX[36] AutoBuild. Initial iodine and holmium heavy atom sites were located in anomalous difference maps calculated in the CCP4[37] package using molecular replacement phases and a holmium derivative data set. The heavy atom sites were refined using the program AutoSHARP[38], and subsequent density modification was performed using RESOLVE[39]. Refinement of the structure was performed by PHENIX[36] Refine and the model was built using COOT[40]. The assignment of ions in the model was aided by appropriate coordination by liganding side chains and anomalous scattering at Cu Kα wavelength (8 keV $f''(I^{2-}) = 6.9e^-$, $f''(Mn^{2+}) = 2.83e^-$, $f''(Ca^{2+}) = 1.3e^-$). The final structural model was refined using data to 2.3 Å with a crystallographic *R*-factor of 20.1% and a free *R*-factor of 22.5% (Supplementary Table 1).

Comparative modelling and structural analysis. A comparative model of Vcx1 in the vacuole-facing conformation was constructed using MODELLER-9V11[41], based on the mjNCX X-ray structure (Protein Data Bank accession 3V5U (ref. 17)). The alignment between the sequences of Vcx1 and mjNCX was obtained by manually editing the alignments from UCSF Chimera[42] and PROMALS3D[43]. The Vcx1 structure and model was analysed and visualized using UCSF Chimera[42] and PyMol[44], and electrostatic surfaces were calculated using APBS[45].

Molecular dynamics simulations. Molecular dynamics simulations were performed with GROMACS4[46], using the CHARMM27[47] all-atom force field and the TIP3P[48] water model. Vcx1 was oriented in an implicit lipid bilayer using PPM[49], then immersed in an explicit 1,2-dimyristoyl-*sn*-glycero-3-phosphocholine (DMPC) lipid bilayer and water using CHARMM-GUI[50]. Periodic boundary conditions and a triclinic box with the volume of 604.326 nm^3 were used. Two independent simulations were carried out, one with and another one without the two Ca^{2+} coordinating Glu 230 and Asp 234 residues. Equilibration was performed by three 10-ns-long runs, gradually increasing the temperature from 100K to 300K, in the canonical (*NVT*) ensemble controlled by the Berendsen[51] thermostat. The positions of non-hydrogen atoms of Vcx1 were restrained by a harmonic potential, with gradually decreasing force constant. A final equilibration step was carried out for 20 ns without restraints, in the isothermal–isobaric (*NpT*) ensemble controlled by the semi-isotropic Berendsen[51] barostat. Each production run was 100 ns long, in the *NpT* ensemble controlled by the Bussi–Donadio–Parrinello[52] thermostat and the semi-isotropic Parrinello–Rahman[53] barostat.

31. Li, M. *et al.* Selecting optimum eukaryotic integral membrane proteins for structure determination by rapid expression and solubilization screening. *J. Mol. Biol.* **385,** 820–830 (2009).
32. Ridilla, M., Narayanan, A., Bolin, J. T. & Yernool, D. A. Identification of the dimer interface of a bacterial Ca^{2+}/H^+ antiporter. *Biochemistry* **51,** 9603–9611 (2012).
33. Grynkiewicz, G., Poenie, M. & Tsien, R. Y. A new generation of Ca^{2+} indicators with greatly improved fluorescence properties. *J. Biol. Chem.* **260,** 3440–3450 (1985).
34. Caffrey, M. & Cherezov, V. Crystallizing membrane proteins using lipidic mesophases. *Nature Protocols* **4,** 706–731 (2009).
35. Kabsch, W. XDS. *Acta Crystallogr. D* **66,** 125–132 (2010).
36. Adams, P. D. *et al.* PHENIX : a comprehensive Python-based system for macromolecular structure solution. *Acta Crystallogr. D* **66,** 213–221 (2010).
37. Winn, M. D. *et al.* Overview of the CCP4 suite and current developments. *Acta Crystallogr.* **67,** 235–242 (2011).
38. Vonrhein, C., Blanc, E., Roversi, P. & Bricogne, G. Automated structure solution with autoSHARP. *Methods Mol. Biol.* **364,** 215–230 (2007).
39. Terwilliger, T. C. Maximum-likelihood density modification. *Acta Crystallogr. D* **56,** 965–972 (2000).
40. Emsley, P. & Cowtan, K. Coot: model-building tools for molecular graphics. *Acta Crystallogr. D* **60,** 2126–2132 (2004).
41. Šali, A. & Blundell, T. L. Comparative protein modelling by satisfaction of spatial restraints. *J. Mol. Biol.* **234,** 779–815 (1993).
42. Pettersen, E. F. *et al.* UCSF Chimera—a visualization system for exploratory research and analysis. *J. Comput. Chem.* **25,** 1605–1612 (2004).
43. Pei, J., Kim, B.-H. & Grishin, N. V. PROMALS3D: a tool for multiple protein sequence and structure alignments. *Nucleic Acids Res.* **36,** 2295–2300 (2008).
44. The PyMOL Molecular Graphics System, Version 1.5.0.4 Schrödinger, LLC.
45. Baker, N. A., Sept, D., Joseph, S., Holst, M. J. & McCammon, J. A. Electrostatics of nanosystems: Application to microtubules and the ribosome. *Proc. Natl Acad. Sci. USA* **98,** 10037–10041 (2001).
46. Hess, B., Kutzner, C., Van der Spoel, D. & Lindahl, E. GROMACS 4: Algorithms for highly efficient, load-balanced, and scalable molecular simulation. *J. Chem. Theory Comput.* **4,** 435–447 (2008).
47. Bjelkmar, P., Larsson, P., Cuendet, M. A., Hess, B. & Lindahl, E. Implementation of the CHARMM force field in GROMACS: Analysis of protein stability effects from correction maps, virtual interaction sites, and water models. *J. Chem. Theory Comput.* **6,** 459–466 (2010).
48. Jorgensen, W. L., Chandrasekhar, J., Madura, J. D., Impey, R. W. & Klein, M. L. Comparison of simple potential functions for simulating liquid water. *J. Chem. Phys.* **79,** 926–935 (1983).
49. Lomize, M. A., Pogozheva, I. D., Joo, H., Mosberg, H. I. & Lomize, A. L. OPM database and PPM web server: resources for positioning of proteins in membranes. *Nucleic Acids Res.* **40,** D370–D376 (2012).

50. Jo, S., Lim, J. B., Klauda, J. B. & Im, W. CHARMM-GUI Membrane Builder for mixed bilayers and its application to yeast membranes. *Biophys. J.* **97,** 50–58 (2009).
51. Berendsen, H. J. C., Postma, J. P. M., Van Gunsteren, W. F., DiNola, A. & Haak, J. R. Molecular dynamics with coupling to an external bath. *J. Chem. Phys.* **81,** 3684–3690 (1984).
52. Bussi, G., Donadio, D. & Parrinello, M. Canonical sampling through velocity rescaling. *J. Chem. Phys.* **126,** 014101–014101–7 (2007).
53. Parrinello, M. & Rahman, A. Polymorphic transitions in single crystals: A new molecular dynamics method. *J. Appl. Phys.* **52,** 7182–7190 (1981).